Giant electromagnetic vortex and MeV monoenergetic electrons generated by short laser pulses in underdense plasma near quarter critical density region

Alexei Zhidkov, Koshichi Nemoto, Takuya Nayuki, Yuji Oishi, and Takashi Fuji
Central Research Institute of Electric Power Industry, 2-6-1 Nagasaka, Yokosuka-shi, Kanagawa-Ken 240-0196, Japan
(Received 9 November 2006; revised manuscript received 6 February 2007; published 5 July 2007)

Very efficient generation of monoenergetic, about 1 MeV, electrons from underdense plasma with its electron density close to the critical, when irradiated by an intense femtosecond laser pulse, is found via two dimensional particle-in-cell simulation. The stimulated Raman scattering of a laser pulse with frequency $\omega \leqslant 2\omega_{\mathrm{pl\,max}}$ gives rise to a giant electromagnetic vortex. In contrast to electron acceleration by the well-known laser pulse wake, injected plasma electrons are accelerated up to vortex ponderomotive potential forming a quite monoenergetic distribution. A relatively high charge of such an electron source makes very efficient generation of soft γ rays with $h\omega > 300$ keV.

DOI: 10.1103/PhysRevE.76.016401 PACS number(s): 52.75.Di, 52.38.Kd, 41.75.Jv

I. INTRODUCTION

The short-pulse-laser-driven acceleration of electrons has been an active area in studying the interaction of laser pulses with both underdense and overdense plasmas. In lower density plasma, acceleration laser wake field order of 100 GV/m and monoenergetic electron bunches up to 1 GeV have been recently observed [1]. In higher density plasma, energetic electrons with moderate energy, usually much less than 1 MeV, have been widely generated to stimulate emission of x rays and the ion acceleration [2]. However, the interaction of intense laser radiation with underdense plasma with its density close to the critical has yet to be studied well. Such a study is brought about by necessity of applications of lower power, tightly focused laser pulses (with a spot size order λ^2) for generation of energetic particles [3], because a lower power laser pulse requires higher plasma density to suppress pulse diffraction.

The interaction of a femtosecond, relativistically intense laser pulse, $a_0 = eE/mc\omega > 1$, where E and ω are the pulse electric field and frequency, with nonuniform underdense plasma near the quarter critical density region may give rise to two well-known processes: the stimulated Raman scattering (SRS) [4,5] and the two-plasmon decay (TPD) [5]. While the TPD process has been studied mostly for overdense plasma irradiated by a long laser pulse, the SRS has been studied in underdense plasma with $\omega_{\mathrm{pl}} \ll \omega$. In contrast to the TPD, the SRS of a short intense laser pulse near the quarter of critical density has an interesting feature: it is a source of excitation of an electromagnetic wave with its frequency less than the plasma frequency. Such an electromagnetic wave cannot propagate inside the plasma (forward SRS) with the maximal density $N_e > N_{\mathrm{cr}}/4$, where $N_{\mathrm{cr}} = m\omega^2/4\pi e^2$ is the critical density, while the plasma is transparent for the laser light. If the SRS appears deeply inside underdense plasma, the wave may not be able to propagate backward (in BSRS) either even in nonuniform plasma if its frequency is lower than a local plasma frequency in an SRS-installed electron density ripple. Hence the SRS pulse can be trapped. A resulting wave is to get a vortexlike structure converting gradually to a plasma electromagnetic soliton or a group of solitons [6–9].

It is known [7] that owing to the frequency downshift accompanying the laser pulse depletion, the condition of soliton formation is met in any uniform underdense plasma. However, if the resonance condition $\omega = 2\omega_{\mathrm{pl}}$ is matched for the fundamental laser frequency, the process can strongly affect the electron acceleration since the structure of the laser wake can distinguish from that of the common plasma wave [10]. In Ref. [11], monoenergetic electron bunches with electron energy about 1 MeV have been observed from underdense plasma with the electron density close to the quarter of critical, $N_{\mathrm{cr}}/4$. The plasma has been formed from a foil target with thickness about 10 μm after irradiating by a first femtosecond laser pulse; then the energetic electrons have been generated during the interaction of this small scale, $\sim 100-200$ μm, plasma with a second femtosecond, higher intensity laser pulse. The appearance of such low energy, monoenergetic electron bunches cannot be explained in the frame of the conventional laser wake field acceleration [10]. In this paper, to reveal the process of generation of lower energy monoenergetic electron bunches in plasma with the density $N_e > N_{\mathrm{cr}}/4$ we perform two dimensional (2D), fully relativistic particle-in-cell simulations. We also estimate the efficiency of Bremsstrahlung radiation with photon energy over 300 keV that can be produced by energetic electrons emitted from such plasma.

II. ELECTROMAGNETIC SOLITON IN PLASMA

It is well known that any electron density ripple causes the scattering of laser light. Consequent modulation of the laser light may give rise to an increase in the density ripple provoking instability. This process is called the stimulated Raman scattering. However, it is usually investigated in the approximation $\omega \gg \omega_{\mathrm{pl}}$ [5,6] where $\omega_{\mathrm{pl}} = (4\pi e^2 N_e/m)^{1/2}$. The relativistic hydrodynamics equations that are widely applied to estimate the SRS instability has the following form [8,9,12]:

$$\left(\frac{\partial^2}{\partial t^2} - c^2\nabla^2\right)\vec{A} + c\vec{\nabla}\frac{\partial\varphi}{\partial t} + \frac{4\pi e N_e}{m\gamma}(c\vec{P} + e\vec{A}) = 0,$$

$$\vec{\nabla}^2\varphi + 4\pi e(N_i - N_e) = 0, \quad \mathrm{div}\,\vec{A} = 0,$$

$$\frac{\partial \vec{P}}{\partial t} = \vec{\nabla}(e\varphi - mc\gamma) + \frac{1}{m\gamma}(\vec{P} + e\vec{A}/c) \times \text{curl}\ \vec{P},$$

$$\vec{P} = \vec{p} - e\vec{A}/c; \quad \gamma^2 = 1 + (\vec{P} + e\vec{A}/c)^2/m^2c^2, \tag{1}$$

where $\boldsymbol{A}$ and φ are the vector and scalar potentials, $\boldsymbol{P}$ is the generalized momentum of electrons, N_i and N_e are the ion and electron densities. Ions are supposed to be immovable.

Assuming that an SRS signal is weak, $\vec{A}=\vec{A}_0+\vec{A}_1$; $\vec{A}_1 \ll \vec{A}_0$, where $\boldsymbol{A}_0$ is the pumping laser light with its frequency ω and wave vector $\boldsymbol{k}$, and $\boldsymbol{A}_1$ is the scattering signal with its frequency ω_1 and wave vector $\boldsymbol{k}_1$, one can expand Eqs. (1) to series equations,

$$\left(\frac{\partial^2}{\partial t^2} - c^2\nabla^2\right)\vec{a}_0 + \Delta^2\vec{a}_0 = 0;$$

$$\Delta^2 = \frac{\omega_{pl}^2}{\sqrt{1+|a_0|^2/2}}, \quad \vec{a}_i = \frac{e}{mc^2}\vec{A}_i;$$

$$\left(\frac{\partial^2}{\partial t^2} - c^2\nabla^2 + \Delta^2\right)\vec{a}_1 = -\delta N\Delta^2\vec{a}_0 + (\vec{a}_0\vec{a}_1)\Delta^2\vec{a}_0/(1+|\vec{a}_0|^2/2);$$

$$\left(\frac{\partial^2}{\partial t^2} + \Delta^2\right)\delta N = c^2/(1+|\vec{a}_0|^2/2)\nabla^2(\vec{a}_0\vec{a}_1). \tag{2}$$

Equations (2) are commonly used for estimation of the SRS instability [4]. In uniform plasma a solution of Eq. (2) in the form of wave $\sim\exp(i\boldsymbol{k}_1\boldsymbol{r}-i\omega_1 t)$ for $\boldsymbol{a}_1$ requires the matching conditions $\boldsymbol{k}_1=\boldsymbol{k}-\boldsymbol{k}_{pl}$, $\omega_1=\omega-\omega_{pl}$, and $\omega^2=(c\boldsymbol{k})^2+\Delta^2$. The dispersion relation (see Ref. [4]) following from Eq. (2) has no solution with $\text{Re}(\omega_1)>0$ if the plasma frequency ω_{pl} exceeds $\omega/2$. Therefore there is no solution in the form of wave. In nonuniform plasma the scattered backward light can propagate as a wave because the local plasma frequency may be less than ω_1. However, the scattered light can induce a density ripple with local plasma frequency exceeding ω_1 even behind the laser pulse. In that case the scattered light cannot propagate backward as a simple wave too.

A solution of Eq. (1) that is valid in the case of $\omega_{pl} > \omega/2$ has been found in Ref. [8] for a circularly polarized pulse in 1D approximation. This solution is an electromagnetic soliton:

$$A_x = 0; \quad A_y + iA_z = a(\chi - u\tau)\exp\{i\Omega[(1-u^2)\tau - u(\chi - u\tau)]\};$$

$$P_x = mcuF(\chi - u\tau); \quad P_y = P_z = 0; \quad u = V/c;$$

$$\Omega = \omega_{soliton}/\omega_{pl}; \quad \tau = \omega_{pl}t; \quad \chi = \omega_{pl}x/c,$$

where V is the velocity of the soliton, $F(\chi-u\tau)$ and $a(\chi-u\tau)$ arbitrary functions. An important fact is that the longitudinal electron momentum depends on the soliton velocity; for very slow soliton $V \ll c$, the electrons in the soliton move in transverse directions. In that case according to Ref. [8] for $V=0$,

$$\vec{A} = \frac{mc^2}{e}\frac{2\sqrt{1-\Omega^2}\cosh(\chi\sqrt{1-\Omega^2})}{\cosh^2(\chi\sqrt{1-\Omega^2}) + \Omega^2 - 1}\exp(i\Omega t);$$

$$\vec{p}_\perp = e\vec{A}/c, \quad \vec{p}_l = 0, \quad \chi = \frac{\omega_{pl}x}{c}. \tag{3}$$

However, these solutions do not include the pumping wave; therefore the determination of the soliton amplitude and frequency Ω requires a numerical simulation. It is apparent that in nonuniform plasma a soliton can appear if $\omega_{pl}N_e\sqrt{1-\Omega^2}/(cdN_e/dx) \gg 1$.

Along with the frequency downshift the SRS and TPD lead to the generation of 2ω and $3\omega/2$ harmonics. Since the condition of the constant vortex, $\text{curl}\boldsymbol{P}=\text{const}$, following from Eq. (1) (see Refs. [8,9]) should be valid for these harmonics as well, the formation of the soliton must be accompanied by higher frequency spherical waves.

The effect of vortex formation on the energy distribution of plasma electrons is not apparent. An important fact is that the longitudinal momentum of electron fluid inside the soliton is zero (in contrast to the electron momentum in the conventional plasma wave) while outside it is not small. It is also clear that all electrons moving towards the soliton with their longitudinal velocity higher than V can be trapped or injected to the soliton field. An injected electron will be accelerated up to the energy

$$\varepsilon = e\int_{x_S}^{\infty} dxE_x = mc\omega_{pl}\int_{x_S}^{\infty} dx\frac{2(1-\Omega^2)^{3/2}\sinh(\xi)\cosh(\xi)}{[\cosh^2(\xi)+\Omega^2-1]^2},$$

$$\xi = \frac{\omega_{pl}}{c}(x - x_S)\sqrt{1-\Omega^2},$$

where we use the longitudinal field of 1D soliton from Ref. [8], see also [13,14]. After evaluating this integral one can get $\varepsilon = 2mc^2(1/\Omega^2 - 1)$. According to this estimation, the energy of accelerated electrons depends only on the ratio of soliton and plasma frequencies that may weakly depend on plasma parameters; all injected electrons may acquire the same energy and hence can form a quite monoenergetic distribution.

III. PIC SIMULATION

In the present paper we performed fully relativistic 2D PIC simulations to study effects of soliton formation on the electron energy distribution. The code employs the "moving window" technique [15]. Plasma parameters are chosen to be close to those in Ref. [11]. The initial electron density profile is shown in Fig. 1, where the electron density linearly decreases at vacuum-plasma interface at the distance 150 μm in both sides; the total plasma length is 350 μm. The maximal electron density is varied from $N_{emax}=10^{20}$ cm^{-3} ($N_e/N_{cr}=0.06$) to $N_{emax}=10^{21}$ cm^{-3} ($N_e/N_{cr}=0.6$). An s-polarized laser pulse $\lambda=0.8$ μm with 30 fs duration (full width at half maximum) is focused on the interface with the spot size of 10 μm diameter and the laser intensity of 5×10^{18} W/cm^2 ($a_0=1.4$) and 5×10^{19} W/cm^2 ($a_0=4.2$). The

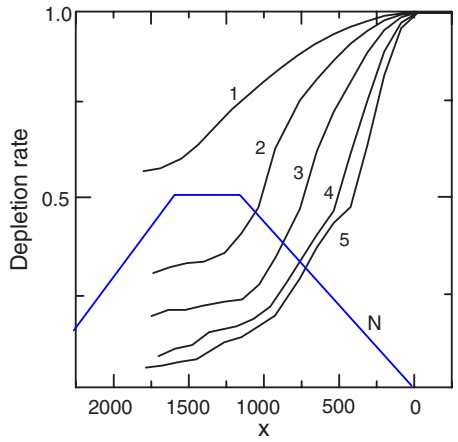

FIG. 1. (Color online) Depletion rate of the laser pulse with intensity $I=5\times10^{18}$ W/cm^2 and duration $\tau=32$ fs in the plasma with the maximal electron density $N_{emax}=1\times10^{20}$ (1), $N_{emax}=2\times10^{20}$ (2), $N_{emax}=4\times10^{20}$ (3), $N_{emax}=8\times10^{20}$ (4), $N_{emax}=1.2\times10^{21}$ (5) cm^{-3}. The trapezoid is the plasma density profile. All coordinate axes are given in $k=c/\omega$ unit.

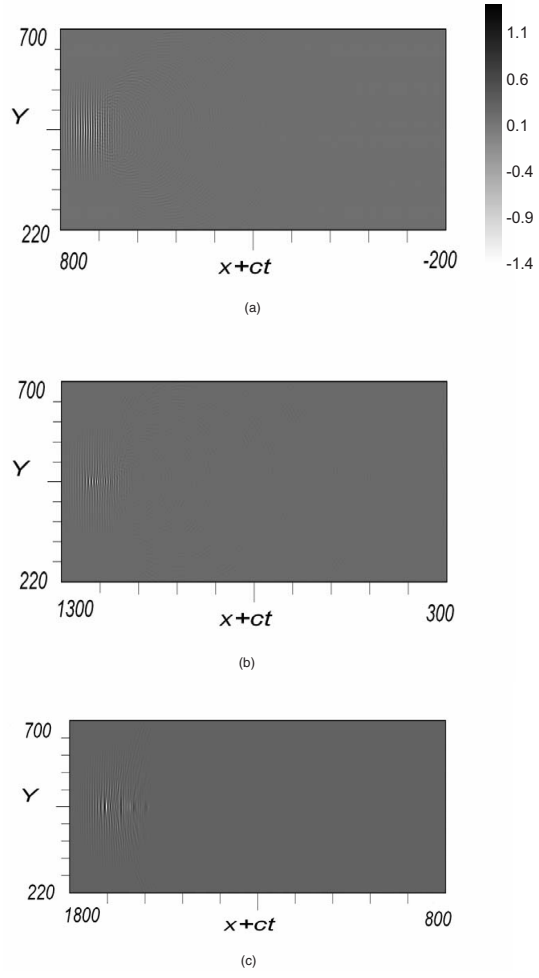

FIG. 2. Transverse component of the electric field in the plasma with $N_{emax}=1\times10^{20}$ cm^{-3} at $\omega t=1000$ (a), 1500 (b), 2000 (c) (high contrast).

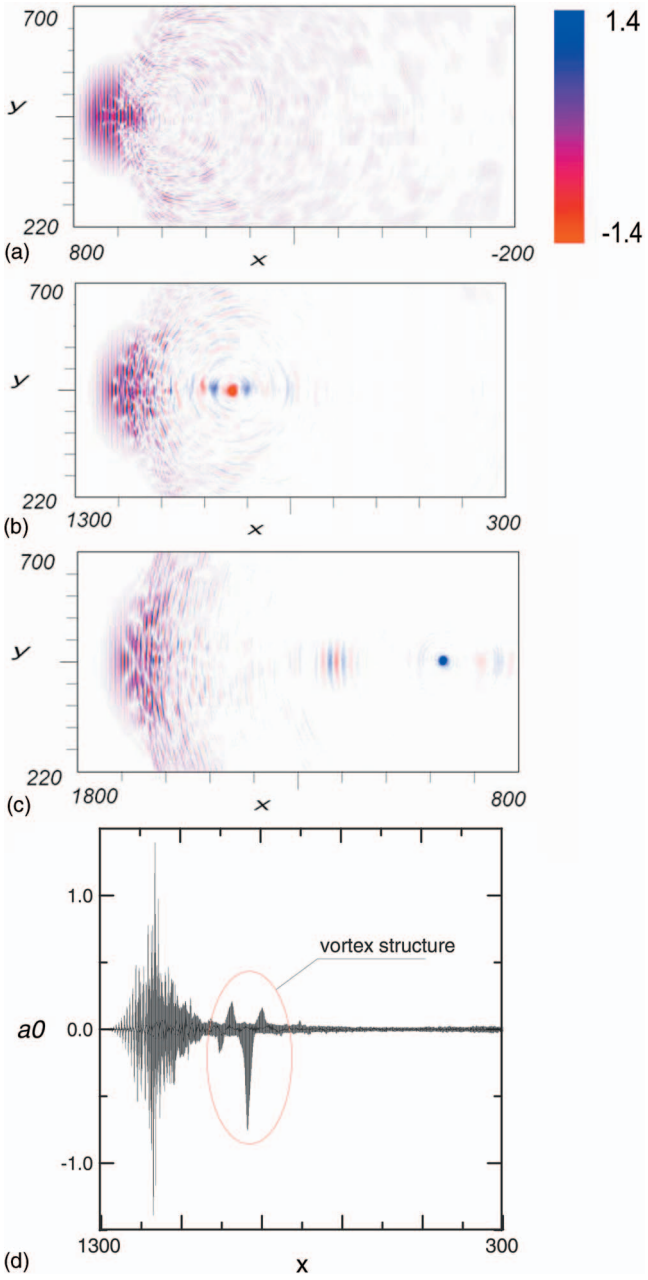

FIG. 3. (Color) Transverse component of the electric field in the plasma with $N_{emax}=2\times10^{20}$ cm^{-3} at $\omega t=1000$ (a), 1500 (b), 2000 (c) (high contrast); the vortex electric field structure near the laser axis at $\omega t=1500$ is given in one dimension (d).

size of the window, moving at the speed of light in vacuum, is 160×120 μm (2800×2048 cells), and we use 16 particles per cell. The laser pulse propagates from the right to the left. No plasma ionization is included.

Temporal evolution of laser pulse depletion is shown in Fig. 1 for different densities of plasma electrons; it changes when the plasma density exceeds $N_e=10^{20}$ cm^{-3}. The depletion can be characterized by two parameters: by a position in plasma where 50% of the laser energy is absorbed and by the slope of depletion rate. The latter characterizes the absorption length. One can see that with higher plasma density, the absorption length becomes shorter, and 50% of the laser en-

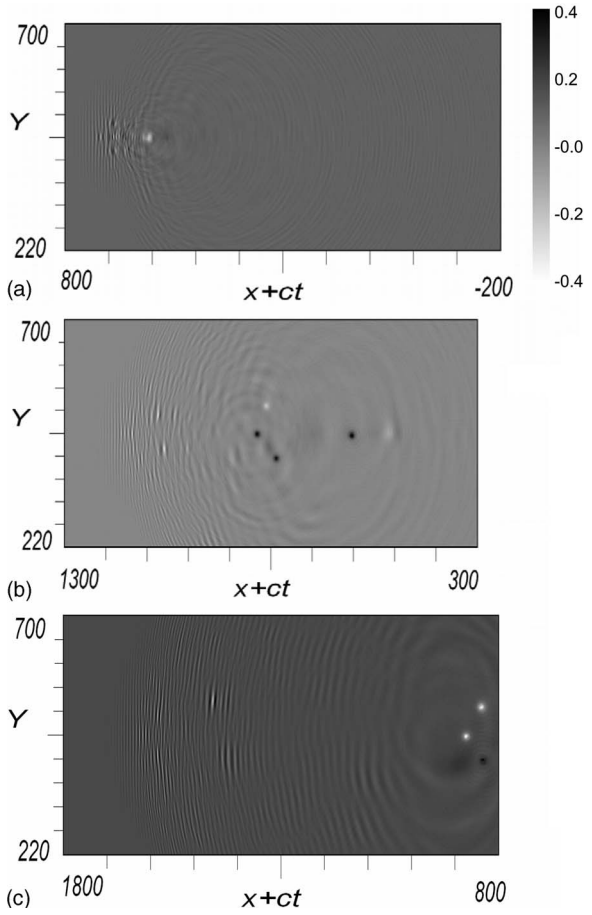

FIG. 4. Transverse component of the electric field in the plasma with $N_{emax}=4\times10^{20}$ cm^{-3} at $\omega t=1000$ (a), 1500 (b), 2000 (c) (high contrast).

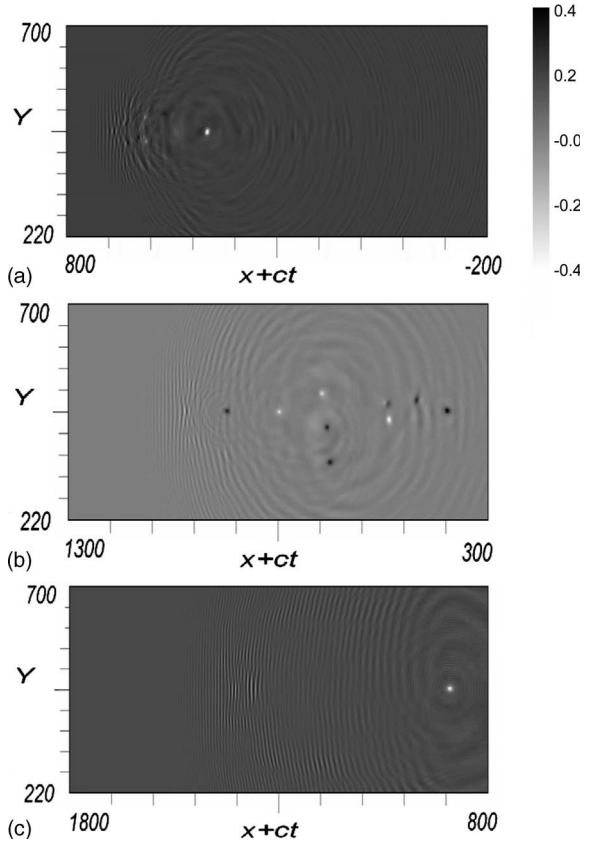

FIG. 5. Transverse component of the electric field in the plasma with $N_{emax}=8\times10^{20}$ cm^{-3} at $\omega t=1000$ (a), 1500 (b), 2000 (c) (high contrast).

ergy is deposited closer to the vicinity of the quarter critical density. For the highest density, the 50% of the laser energy is absorbed in approximately 30 μm length. Upon dividing the deposited energy by the number of particles that absorb this energy one can find the particle temperature which is close to $T\sim0.5$ MeV for the laser intensity $I=5\times10^{18}$ W/cm^2. We attribute this strong absorption of the laser energy in the vicinity of the quarter of critical density to the SRS and TPI effects.

The spatial distribution of the z component of the electric field that is initially equal to the laser field is given in Figs. 2–5 for different times and for different plasma densities. The contrast in the figures is increased to show the scattered and diffracted light. As seen in Fig. 2, if the density of plasma is not high, $N_{emax}=10^{20}$ cm^{-3}, the behavior of the laser field including self-focusing [Fig. 2(b)] is very common. Although the laser filamentation appears [Fig. 2(c)], the laser pulse leaves the plasma slab before the formation of any soliton. Very different dynamics of the laser pulse is observed for higher density, $N_{emax}=2\times10^{20}$ cm^{-3}, even though the maximal density is smaller than the quarter of the critical. Initially, the common self-focusing is clearly seen (Fig. 3). Along with the self-focusing, the ponderomotive force of the laser pulse makes a density ripple at the front of the pulse. When electron density in the ripple exceeds the quarter of the critical the strong SRS and TPI appear. The field strength of the scattered light as shown in Fig. 3(b) is comparable to the laser field and is strong enough to make a density ripple behind. An intense vortex structure moving with velocity much lower than the speed of light is generated as a result. The field distribution in the structure differs from that given by Eq. (3). However, after a while, a pure soliton is extracted from the structure as shown in Fig. 3(c). Behind the laser pulse the density ripple soon disappears, and the radiation with $\omega'=\omega-\omega_{pl}$ can propagate inside the plasma with a lower group velocity. This wave is seen in Fig. 3(c) in the front of the soliton. A similar scenario is observed initially for the higher density $N_{emax}=4\times10^{20}$ cm^{-3} (see Fig. 4). However, the vortex structure falls into four solitons as shown in Fig. 4(b). This confirms a weak dependence of the soliton amplitude on the plasma parameters. When the higher energy is deposited in plasma more solitons with approximately the same energy appear. With the further density increase, $N_{emax}=8\times10^{20}$ cm^{-3}, as shown in Fig. 5, an intense vortex structure appears in the vicinity of a quarter of the critical density again. Since the laser energy is deposited in a shorter distance, eight solitons are formed as shown in Fig. 5(b). One also can see quite a strong harmonic at the double frequency accompanying the lower frequency vortex generation. This wave also acquires a group velocity much less than the speed of light, therefore it is a cylindrical wave as shown in Figs. 3–5. We do not observe a z component of $3\omega/2$ harmonics here.

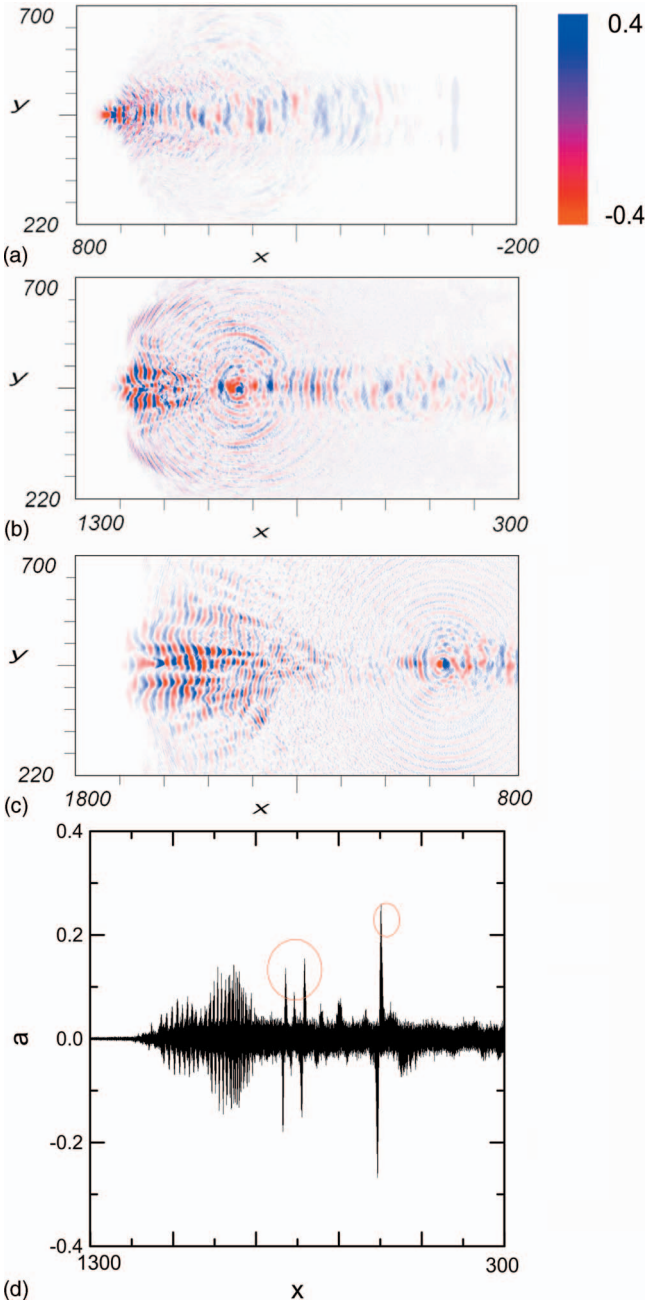

FIG. 6. (Color) X component of the electric field in the plasma with $N_{emax}=2\times10^{20}$ cm^{-3} at $\omega t=1000$ (a), 1500 (b), 2000 (c); 1D plot of the field near the laser axis at $\omega t=1500$ (d).

Spatial distribution of the longitudinal component of the electric field for different plasma densities $N_{emax}=(2-8)\times10^{20}$ cm^{-3} is shown in Figs. 6–8. The formations of the vortex structure are clearly seen. These vortexes spatially correlate with those given in Figs. 2–5 being part of the same structure. However, this component of the vortex does not convert to the complete soliton mode in the calculation time. The result of the laser filamentation is also well seen in the figure; the strongly focused laser filaments generate a longitudinal component. The spectral analysis gives two high frequency harmonics, 2ω and $3\omega/2$, excited in the vicinity of the critical density. Similar to the transverse component,

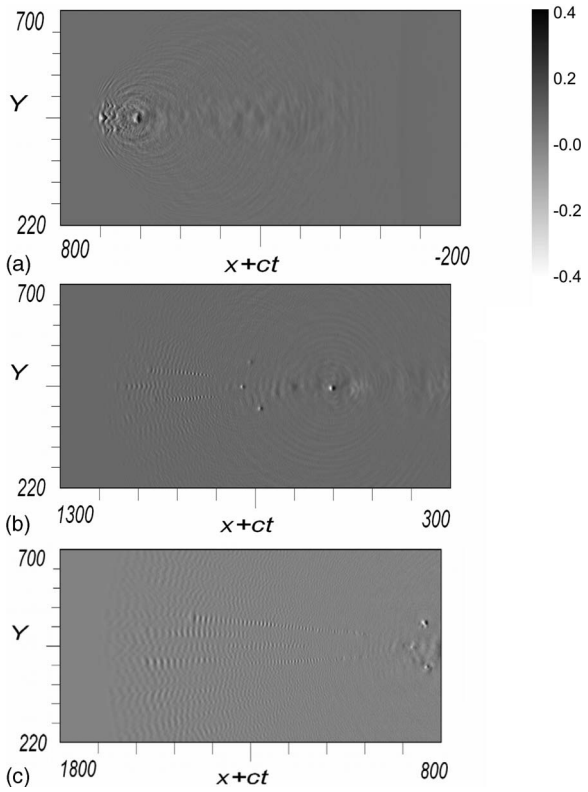

FIG. 7. X component of the electric field in the plasma with $N_{emax}=4\times10^{20}$ cm^{-3} at $\omega t=1000$ (a), 1500 (b), 2000 (c).

these are also spherical waves. The longitudinal component of the electric field has a nonoscillating component inside the solitons. This agrees qualitatively with the 1D approximation [12,13]. Therefore this field can accelerate an electron if it is properly injected.

Spatial distributions of the electron density are presented in Fig. 9. Lower density spots are exposed; their positions

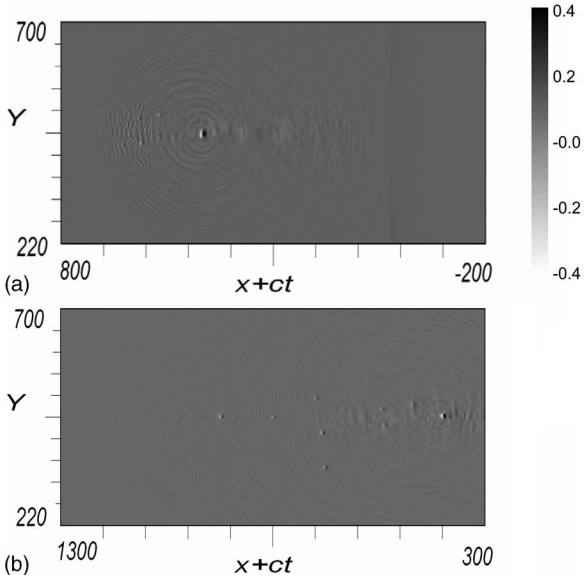

FIG. 8. X component of the electric field in the plasma with $N_{emax}=8\times10^{20}$ cm^{-3} at $\omega t=1000$ (a), 1500 (b).

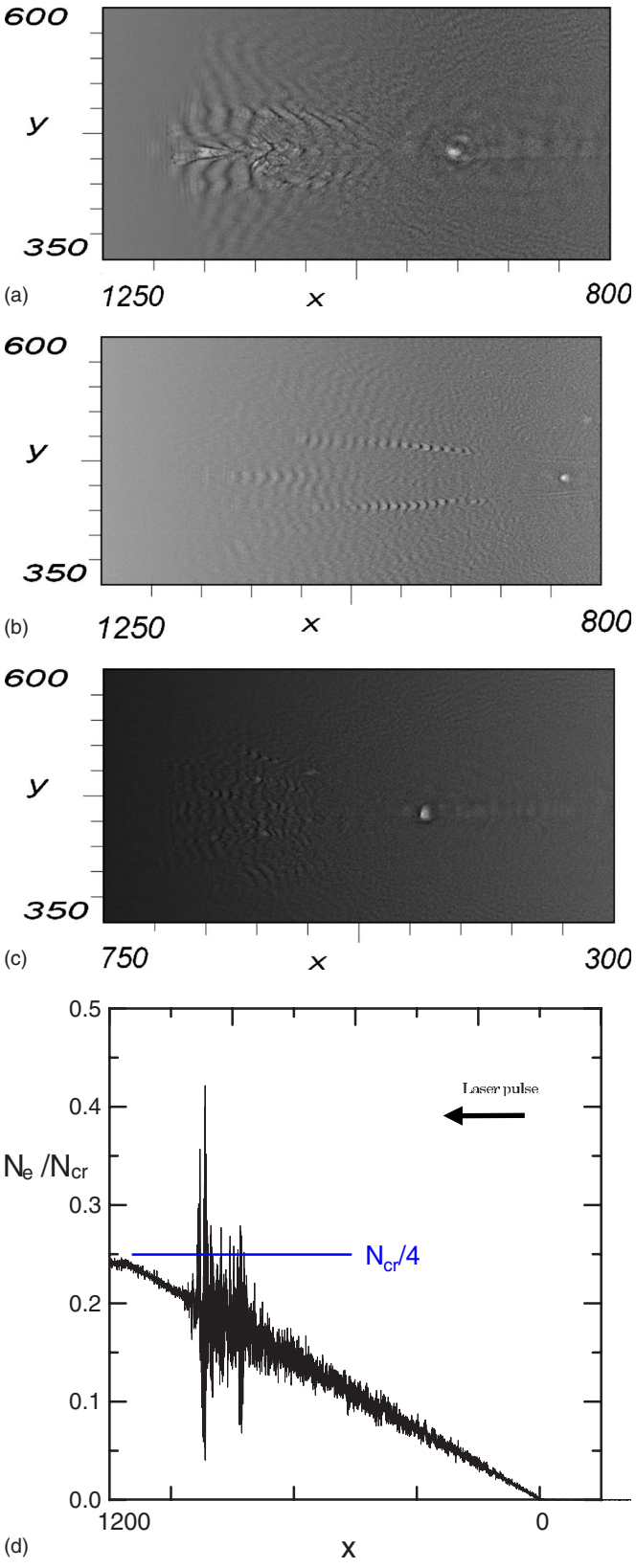

FIG. 9. (Color online) Spatial distribution of electron density in plasma with $N_{emax}=2\times10^{20}$ cm^{-3} (a), $N_{emax}=4\times10^{20}$ (b) at $\omega t=1500$, and $N_{emax}=8\times10^{20}$ at $\omega t=1000$ (c); 1D density distribution near the laser axis at $\omega t=1000$ (the vortex has been formed) for $N_{emax}=4\times10^{20}$ (d); solid line shows the quarter of the critical density.

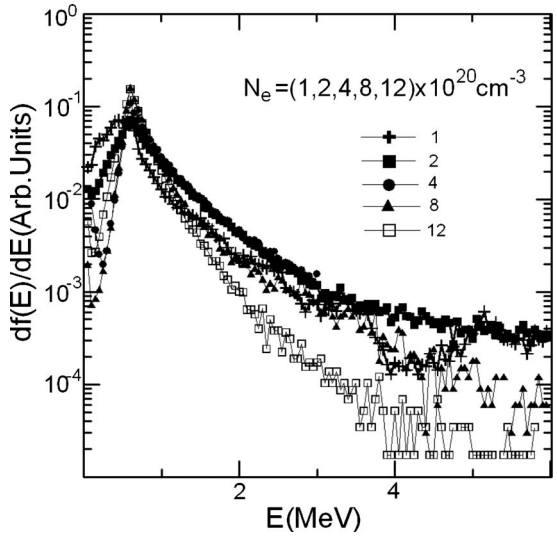

FIG. 10. Electron energy distribution in plasma $N_{emax}=1\times10^{20}$ cm^{-3} (1), $N_{emax}=2\times10^{20}$ (2), $N_{emax}=4\times10^{20}$ (3), $N_{emax}=8\times10^{20}$ (4), $N_{emax}=1.2\times10^{21}$ (5).

correlate with that of solitons. After the soliton is completely formed, its density structure agrees qualitatively with that from the theoretical analysis [8]. In Fig. 9(d), one can determine the position of vortex formation. The initial density in that point is less than a quarter of the critical density. However, owing to the strong ponderomotive force acting forward, the density at the front of the pulse exceeds the quarter of the critical resulting in strong SRS. Then, the scattering light also induces the density modulation behind the pulse with the maximal value exceeding the quarter of the critical; the frequency of the scattered light therefore becomes less than the local plasma frequency and the light cannot propagate in the form of a plane wave.

The calculated distribution function of energetic electron normalized on the plasma density is given in Fig. 10. For the plasma density exceeding the quarter of the critical we observe a very narrow peak in the distribution at the energy about 800 keV. We attribute this peak to the electron acceleration by the soliton longitudinal field while the higher energy tail is the result of acceleration by conventional plasma wave. Since with the density increase a range of the regular plasma wave shortens, the number of higher energy electrons decreases. The efficiency of electron generation is fairly good; for the plasma density $N_{emax}=4\times10^{20}$ cm^{-3} more than 8% of the total laser energy is converted to 1-MeV electrons. In Fig. 11 the energy distribution of the electron emitted from the prepared plasma [11] is given. The scale of the maximal electron density plasma slab is about 100 μm as seen so that parameters in the experiment are close to those used in the simulation. The distribution obtained in the present simulation is in surprisingly good agreement with the experiment.

In Fig. 12 we present the result of calculation of the interaction of much higher intensity laser pulse with the quarter critical density plasma $N_{emax}=4\times10^{20}$ cm^{-3}. One can see that an increase of the deposited energy leads to the formation of a group of solitons that all have very similar param-

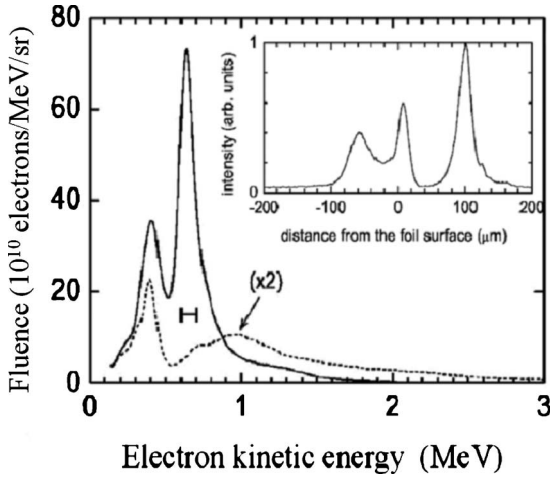

FIG. 11. Electron energy distribution and possible density distribution of prepared plasma in the experiment measured in Ref. [11].

eters. The distribution function of energetic electrons is not so monoenergetic as that for the lower laser intensity, however, the peak energies are very close. The increase of the laser intensity gives an increase of the number of near-1-MeV electrons only. This also goes along with the proposed mechanism of soliton field acceleration.

IV. BREMSSTRAHLUNG RADIATION OF THE ENERGETIC ELECTRONS

The bremsstrahlung radiation in the range of photon energy over 100 keV can be very efficient with a few MeV energy electron beam. The number of photons per one electron with energy E_0 emitted from a thin target in the energy range $\varepsilon-\varepsilon+d\varepsilon$ in the angle θ in the electron propagation has the following form [16]:

$$N(\varepsilon,\zeta)d\varepsilon d\varsigma = \frac{4Z^2NL}{137}\left(\frac{e^2}{mc^2}\right)^2\frac{d\varepsilon}{\varepsilon}\varsigma d\varsigma\frac{4}{(\varsigma^2+1)^4} \times\left[(\varsigma^4+1)\ln\left(\frac{111(\varsigma^2+1)}{Z^{1/3}}\right)-(\varsigma^2-1)^2\right],$$

where ε is a photon energy, $\zeta=E_0\theta/mc^2$ with θ the angle of photon radiation, N and Z are the ion charge and ion density in a target, L is the length of the target. The total number of photons with the energy over 300 keV can be estimated assuming that these photons are not absorbed by the target. This approximation is quite good since the maximal ionization potential is $I=13.6Z^2\sim 100$ keV. Evaluation of the integral over the solid angle gives a constant order of 10 while the integral over the energy gives the slow logarithmic dependence for the number of photons,

$$N(\varepsilon > E_{\min})/N_e = BZ^2NL\left(\frac{e^2}{mc^2}\right)^2\ln(E_0/E_{\min}),\quad B\sim 0.3.$$

For a solid target with $Z>50$ this estimation gives the efficiency over 10%. The calculation with the distribution function shown in Fig. 5 gives very close efficiency.

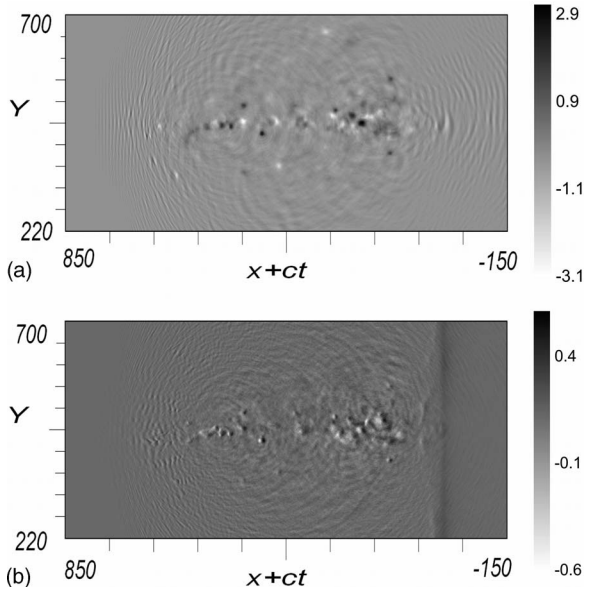

FIG. 12. Transverse (a) and longitudinal (b) component of electric field in plasma with $N_{emax}=4\times10^{20}$ irradiated by the laser pulse with intensity $I=5\times10^{19}$ W/cm^2 at $\omega t=1000$.

V. CONCLUSION

In summary, we have carried out fully relativistic 2D PIC simulations of the interaction of intense femtosecond laser pulses with plasma slabs near the quarter of the critical density to study possible mechanisms of electron acceleration.

In a plasma slab with its density exceeding $N_{emax}=4\times10^{20}$ cm^{-3}, the stimulated Raman scattering leads to the formation of an intense electromagnetic vortex structure (its field strength comparable to the field of the laser pulse). Later the vortex transforms to electromagnetic solitons. A considerable portion of the laser energy is deposited near the quarter of the critical density. Although the two-plasmon decay process plays a role, its contribution is much smaller than the contribution of the SRS.

We also observe a similar process at lower plasma density $N_{emax}=2\times10^{20}$ cm^{-3}. Electron density in the ripple produced by the ponderomotive acceleration of plasma electrons at the front and at the rear of the laser pulse becomes higher than the quarter of the critical, as a result, a strong electromagnetic (EM) vortex is formed as well. Since the density behind the laser pulse is smaller than the quarter of the critical, a portion of the laser energy converted to a plane wave with $\omega'=\omega$-ω_{pl} (local).

The velocity of the EM vortex appears to be less than the velocity of the electron fluid behind the laser pulse. Therefore some of the plasma electrons can be injected in the EM vortex. The energy acquired by such electrons depends only on the vortex amplitude equal to $2mc^2[(\omega_{pl}/\omega_{soliton})^2-1]$ that

weakly depends on the plasma density. We believe this injection and acceleration result in the quite monoenergetic energy distribution of accelerated electrons with their energy about 1 MeV. We have found that about 10% of the laser energy is converted to the electrons with energy in the range of 0.5–1 MeV. The bremsstrahlung radiation of such electron beam with energy exceeding 300 keV can be very efficient, up to 1% of the laser energy.

[1] S. P. D. Mangles *et al.*, Nature (London) **431**, 535 (2004); C. G. R. Geddes *et al.*, *ibid.* **431**, 538 (2004); J. Faure *et al.*, *ibid.* **431**, 541 (2004); W. P. Leemans *et al.*, Nat. Phys. **2**, 696 (2006).

[2] Z. Li *et al.*, Phys. Plasmas **13**, 043104 (2006); H. Teng, J. Zhang, Z. L. Chen, Y. T. Li, K. Li, X. Y. Peng, and J. X. Ma, Phys. Rev. E **67**, 026408 (2003); Y. T. Li, X. H. Yuan, M. H. Xu, Z. Y. Zheng, Z. M. Sheng, M. Chen, Y. Y. Ma, W. X. Liang, Q. Z. Yu, Y. Zhang, F. Liu, Z. H. Wang, Z. Y. Wei, W. Zhao, Z. Jin, and J. Zhang, Phys. Rev. Lett. **96**, 165003 (2006); A. Zhidkov, A. Sasaki, T. Utsumi, I. Fukumoto, T. Tajima, F. Saito, Y. Hironaka, K. G. Nakamura, K.-i. Kondo, and M. Yoshida, Phys. Rev. E **62**, 7232 (2001).

[3] T. Nayuki, T. Fuji, Y. Oishi, K. Nemoto, and X. Wang, Rev. Sci. Instrum. **76**, 073305 (2005).

[4] A. S. Sakharov and V. I. Kirsanov, Phys. Rev. E **49**, 3274 (1994); W. B. Mori, C. D. Decker, D. E. Hinkel, and T. Katsouleas, Phys. Rev. Lett. **72**, 1482 (1994); Phys. Plasmas **3**, 1360 (1996).

[5] T. M. Antonsen and P. Mora, Phys. Fluids B **5**, 1440 (1993); W. Seka *et al.*, *ibid.* **4**, 2232 (1991).

[6] A. G. Litvak, Sov. Phys. JETP **3**, 696 (1970); V. A. Kozlov, A. G. Litvak, and E. V. Suvorov, *ibid.* **49**, 75 (1979).

[7] S. V. Bulanov, I. N. Inovenkov, V. I. Kirsanov, N. M. Naumova, and A. S. Sakharov, Phys. Fluids B **4**, 1935 (1992).

[8] T. Z. Esirkepov, F. F. Kamenetz, S. V. Bulanov, and N. M. Naumova, JETP Lett. **68**, 36 (1998).

[9] S. V. Bulanov, T. Z. Esirkepov, N. M. Naumova, F. Pegoraro, and V. A. Vshivkov, Phys. Rev. Lett. **82**, 3440 (1999); Y. Sentoku, T. Z. Esirkepov, K. Mima, K. Nishihara, F. Califano, F. Pegoraro, H. Sakagami, Y. Kitagawa, N. M. Naumova, and S. V. Bulanov, *ibid.* **83**, 3434 (1999); N. M. Naumova *et al.*, Phys. Plasmas **8**, 4149 (2001).

[10] T. Tajima and J. M. Dawson, Phys. Rev. Lett. **43**, 267 (1979).

[11] X. Wang, K. Nishikawa, and K. Nemoto, Phys. Plasmas **13**, 080702 (2006).

[12] S. V. Bulanov, F. Califano, T. Z. Esirkepov, K. Mima, N. M. Naumova, K. Nishihara, and F. Pegoraro, Physica D **152-153**, 682 (2001); D. Farina and S. V. Bulanov, Plasma Phys. Rep. **27**, 641 (2001); Phys. Rev. Lett. **86**, 5289 (2001); Plasma Phys. Controlled Fusion **47**, A73 (2005); S. V. Bulanov and F. Pegoraro, Phys. Rev. E **65**, 066405 (2002); T. Esirkepov, K. Nishihara, S. V. Bulanov, and F. Pegoraro, Phys. Rev. Lett. **89**, 275002 (2002); M. Lontano, M. Borghesi, S. V. Bulanov, T. Z. Esirkepov, D. Farina, N. Naumova, K. Nishihara, M. Passoni, F. Pegoraro, H. Ruhl, A. S. Sakharov, and O. Willi, Laser Part. Beams **21**, 541 (2003).

[13] G. Lehmann, E. W. Laedke, and K. H. Spatschek, Phys. Plasmas **13**, 092302 (2006).

[14] A. Macic, L. Hadzievski, and M. Scoric, Phys. Plasmas **13**, 052309 (2006); B. Li, S. Ishiguro, M. M. Scoric, and T. Sato, *ibid.* **13**, 042303 (2006); **12**, 103103 (2005).

[15] A. Zhidkov, J. Koga, T. Hosokai, K. Kinoshita, and M. Uesaka, Phys. Plasmas **11**, 5379 (2004).

[16] L. I. Schiff, Phys. Rev. **83**, 252 (1951); A. L. Pokrovsky, A. E. Kaplan, and P. L. Shkolnikov, J. Appl. Phys. **100**, 044328 (2006).